Pergamon

NanoStructured Materials, Vol. 11, No. 8, pp. 1245–1251, 1999
Elsevier Science Ltd

0965-9773/99/$–see front matter

PII S0965-9773(99)00415-8

# COMPOSITIONAL PARTITION IN Ag-Nb ALLOY CLUSTERS PRODUCED BY A PLASMA-GAS-CONDENSATION CLUSTER SOURCE

K. Wakoh*, T. Hihata**, D.L. Peng** and K. Sumiyama*
*Institute for Materials Research, Tohoku University, Sendai 980-8577, Japan
**CREST, Japan Science and Technology Corporation (JST),
Kawaguchi 332-0012, Japan

(Received September 27, 1999)
(Accepted November 5, 1999)

**Abstract**—We have produced Ag-Nb clusters by a facing-target type plasma-gas-condensation cluster source as our first step toward alloy cluster formation. The Ag-Nb clusters have been deposited on substrates and examined by a transmission electron microscope with a nano-beam energy dispersive X-ray analysis. We have obtained Ag-Nb alloy clusters with the sizes range between 5 and 10 nm in diameter. Their chemical compositions are broadly dispersed and partitioned into Ag-rich and Nb-rich ones, being consistent with the immiscible type equilibrium phase diagram. This result suggests that alloy cluster formation is driven by the alloy phase stability. *©2000 Acta Metallurgica Inc.*

## Introduction

A great deal of interest has been concentrated on nano-scale heterogeneous materials such as nano-crystalline and granular materials (1) because their physical and chemical properties are significantly different from homogeneous counterparts. These materials have been mainly obtained by precipitation of small crystallites in a matrix via low temperature heat treatment of supersaturated precursors which are prepared by vapor-, liquid-, and solid-quenching methods. Small particles and clusters have been also candidate precursors to obtain such structure-controlled materials in nanometer scale (2–4). Since they have the unique structures and properties owing to their nanometer sizes (4–7), it has been desired to fabricate particle- or cluster-assembled materials (2,4). In order to optimize their properties, we need size-selected clusters as building blocks. For the first step, we have recently constructed plasma-gas-condensation (PGC) type cluster deposition apparatus (7–9), which is similar to the one originally developed by Haberland *et al*. (11,12). This is a combination of sputter vaporization and inert gas condensation techniques, that enables one to vaporize refractory metals. The clusters formed in our source are extracted through a nozzle into a better vacuum chamber in order to prevent further cluster growth and to control their size. Hence, we have obtained monodispersed clusters, whose mean sizes are controllable between 3 and 13 nm in diameter.

As the next step of this approach, we wished to produce alloy clusters, because the alloying behavior in the nanometer sized clusters has been an interesting subject: atom-atom bonding natures are different from those of bulk solids (13–15), and diffusion and mixing are very fast in the atomic scale (16,17). We tried to set up a very simple PGC-type cluster source and examined how we could control the chemical compositions of clusters. This paper deals with a preliminary result on the chemical fluctuation of Ag-Nb clusters formed

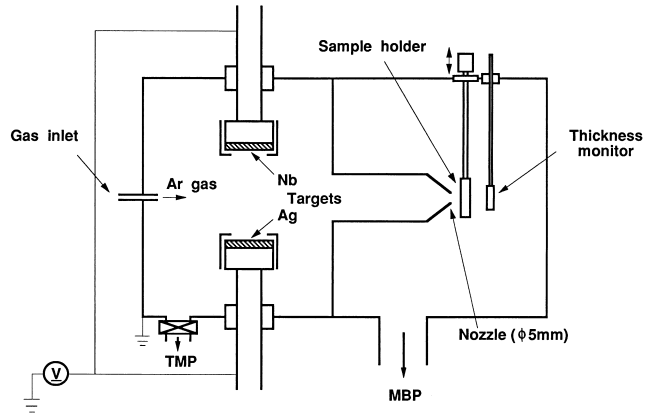


Figure 1. Schematic drawing of the present PGC-type cluster deposition apparatus. TMP and MBP represent turbo-molecular pump and mechanical booster pump, respectively.

in this cluster source, where the alloy system is immiscible in the equilibrium state (18). We emphasize that the alloy phase stability is one of the key parameters in the alloy cluster formation.

## Experimental

As schematically shown in Figure 1, we used the facing target type dc sputtering source, which was a combination of a hollow cathode discharge mode and a magnetron mode to attain high density metal vapor. We could get a high ionization efficiency of Ar and thus a high sputtering rate owing to the magnetic field applied perpendicular to the surfaces of two targets. In the present study, Ag and Nb targets of 50 mm in diameter were set up for alloy cluster formation. The distance between the targets was 100 mm. The Ar gas stream adjusted by a fine mass flow controller was injected steadily through a gas inlet located at the backside of the source. The electric power was supplied independently for these two targets to control the chemical composition of individual elements. Clusters nucleate in a high pressure Ar gas atmosphere (0.2–0.4 kPa) and grow in the space between the target and the nozzle (growth region). The cluster beam was extracted through the nozzle of 5 mm in diameter by a mechanical booster pump. The operational pressure was about $1 \times 10^1$ Pa in the deposition chamber.

The deposition rate was measured by a quartz oscillator-type thickness monitor. For transmission electron microscope (TEM) observation, the microgrid, which is a carbon-coated colodion film supported by a Cu grid, was used as a substrate. The samples were exposed in air for transportation and observed with the Hitachi HF-2000 electron microscope, operating at 200 kV. The chemical compositions of the clusters were measured by a nano-beam energy dispersive X-ray (EDX) analysis using a detector installed on the TEM. The TEM images were taken as digitized data with a slow-scan charge coupled device (CCD) camera.

## Results

Figure 2(a) shows a typical bright-field TEM image of the Ag-Nb clusters prepared at $R_{Ar} = 1.0 \times 10^{-3}$ mol/s (1300 sccm, standard cubic centimeter per minute), $p_s = 400$ Pa, $P_{Ag} = 100$ W, and $P_{Nb} = 200$ W. Here, $R_{Ar}$ is the flow rate of Ar gas, $p_s$ the inert-gas pressure in the cluster source, $P_{Ag}$ the sputtering power for the Ag target, and $P_{Nb}$ that for the Nb target. The EDX spectrum taken with a spread beam

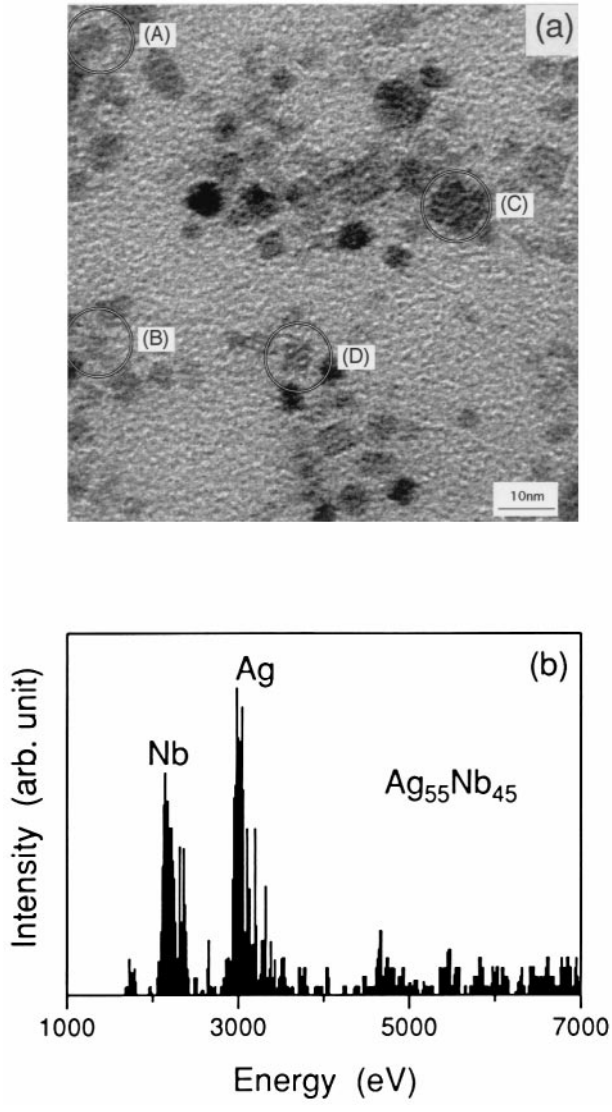


Figure 2. (a) A bright-field TEM image of Ag-Nb clusters and (b) an EDX spectrum of the average composition (45 at.% Nb) taken with a spread beam of about 0.3 $\mu$m.

of about 0.3 $\mu$m is shown in Figure 2(b). The mean composition estimated from Figure 2(b) is about 45 at.% Nb.

Figure 3(a) shows a bright-field TEM image of the Ag-Nb clusters prepared at $R_{Ar} = 1.0 \times 10^{-3}$ mol/s, $p_s = 400$ Pa, $P_{Ag} = 100$ W, and $P_{Nb} = 200$ W. Many clusters are roughly spherical and dispersed uniformly in the size range between 5 and 10 nm. Cubic shape clusters with faceted surfaces are also seen. Figure 3(b) shows the electron diffraction pattern of the present sample. The diffraction rings are assigned to two sets of f.c.c. type structures with the lattice parameters $a =$ 0.41 and 0.44 nm. Since the lattice constant, $a = 0.409$ nm for f.c.c. Ag and 0.442 nm for NaCl-type Nb(NO) (19), these two f.c.c. phases can be attributed to an Ag-based alloy and an

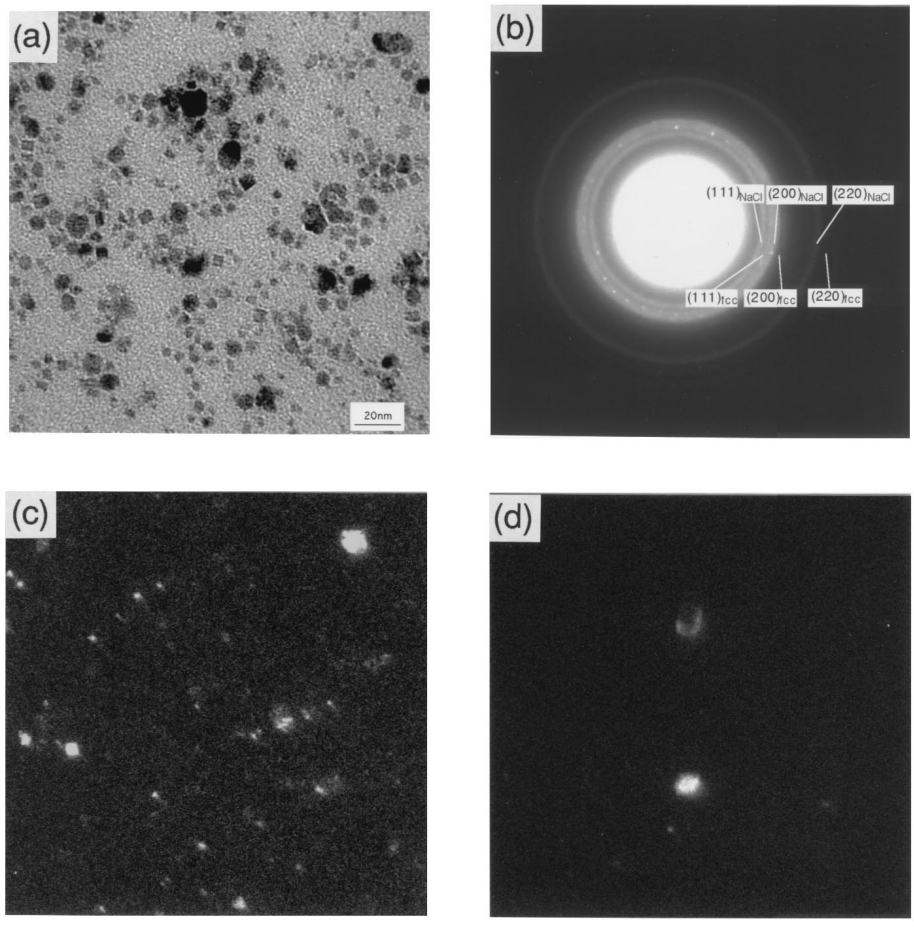


Figure 3. (a) A bright-field TEM image and (b) an electron diffraction pattern of Ag-Nb clusters. (c) and (d) are dark-field TEM images of the same area as the photograph (a) with the objective aperture covering a part of the $(111)_{fcc}$ ring and the $(111)_{NaCl}$ ring, respectively. They correspond to (c) Ag-rich and (d) Nb-rich clusters.

Nb(NO)-based compound. This result suggests that Nb-vapor atoms easily react with $O_2$ and $N_2$ in the present low vacuum condition of the deposition chamber during the operation. Figures 3(c) and (d) are dark-field TEM images of the same area as Figure 3(a) with the objective aperture covering a part of the $(111)_{fcc}$ ring with $a = 0.41$ nm and that of the $(111)_{NaCl}$ ring with $a = 0.44$ nm, respectively. These results suggest that an individual cluster has a unique crystal structure.

Figure 4 shows the nano-electron beam EDX spectra taken from the labeled clusters A to D in Figure 2(a). We randomly selected 25 different clusters and took the EDX spectra by nano-electron beams. The estimated compositions are shown as a histogram in Figure 5. The chemical compositions of these clusters are widely distributed and exhibit two peaks in the Ag-rich and Nb-rich sides. The average composition of the histogram is about 45 at.% Nb being consistent with the EDX spectrum taken with the spread beam (Figure 2(b)).

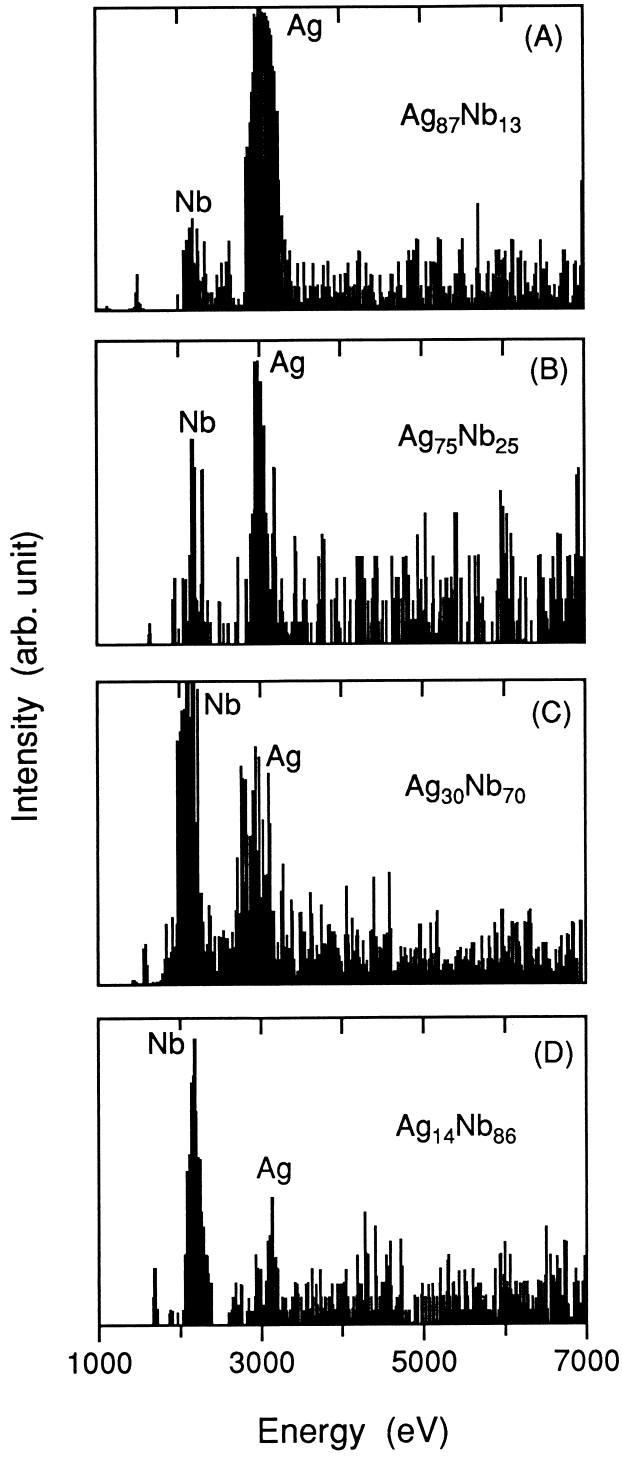


Figure 4. Nano-beam EDX spectra taken from the small areas of about 10 nm as indicated by the labels A to D in Figure 2(a).

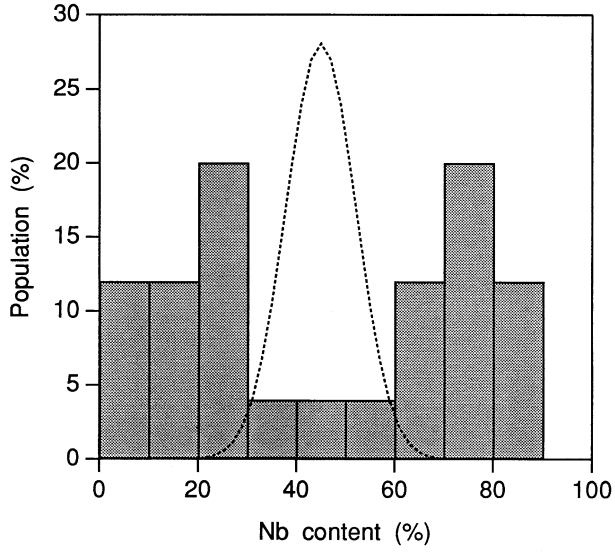


Figure 5. A chemical composition histogram evaluated from the nano-beam EDX spectra of 25 clusters. The dotted line indicates a binomial distribution for 45 at.% Nb.

## Discussion

In the inert gas condensation process, vaporized metal atoms from the targets rapidly loose their kinetic energy by collisions with the inert gas atoms. The first stage of the cluster growth is embryo formation by thermodynamical fluctuation through three-body collisions (5). This stage probably takes place in front of the sputtering target. These embryos are so small that they easily evaporate instead of growing to larger clusters. When they stoichastically become larger than the critical size, the cluster growth is promoted as predicted in the classical nucleation and growth theory (10): such a cluster grows step by step with absorption of atoms arriving at the surface. On the TEM microgrid, we observed nanometer sized clusters consisting of about $1 \times 10^4$ atoms which had been produced via a large number of cluster-atom and cluster-cluster collisions.

In the PGC cluster source, the cluster size depends on the length of the growth region. With moving the sputtering target to change the length of the growth region in the PGC cluster source, we measured the mass distribution of the Nb clusters by a time-of-flight high-mass spectrometer (10,20). This result indicated that the small clusters containing less than 200 atoms were mainly formed at the 50 mm distance from the target, corresponding to the middle point of the Ag and Nb targets in the present apparatus. Although Nb-rich clusters form an Nb(NO)-based compound phase, we simply take into account of mixing and reaction between Nb and Ag atoms. Provided that the Nb and Ag clusters consisting of about 200 atoms meet at the center position between the sputtering targets, they collide each other and form larger clusters. In the random collision and coalescence process, the compositional distribution of the Ag-Nb clusters, *I(m,N)*, as a function of Nb content, *m/N* ($m = 0, 1, 2, \ldots, N$), should be binomial as follows,

$$I(m, N) = \frac{N!}{(N - m)!m!}(1 - x)^{N-m}x^m, \quad (1)$$

where $N$ is collision times and $x$ the partial molar ratio. Here, we assumed $x = 0.45$ because the average composition taken by a spread beam EDX was almost 45% Nb. The binomial distribution obtained for $N = 50$ is shown in Figure 5 by the broken line, being inconsistent with the experimental result.

The dark-field TEM images (Figures 3(c) and (d)) and the chemical analyses (Figure 4) demonstrate that the individual cluster has the unique crystal structure depending on their chemical compositions, i.e., f.c.c. in the Ag-rich clusters or NaCl-type in the Nb-rich ones. Based upon the immiscible type equilibrium phase diagram of Ag-Nb, the formation of the Ag-rich and Nb-rich clusters suggests that random reaction between Ag and Nb atoms and coalescence of their clusters are markedly suppressed due to their positive formation enthalpy. In the initial growth stage, reevaporation of Ag atoms (Nb atoms) from Nb-rich cluster (Ag-rich cluster) is plausible, because Ag-Nb chemical bonding is much weaker than Ag-Ag or Nb-Nb one. Consequently, Ag- and Nb-rich clusters containing their partner elements are formed to be metastable primary solid solutions as seen in Figure 5. This feature probably originates from the compositional partition which is expected from the equilibrium phase diagram (18). In order to minimize reactions of metal atom with $O_2$ and $N_2$, we are preparing a deposition chamber with a much better vacuum condition. Finally, it is worth mentioning the results of Co-Al alloy cluster formation by the similar preparation method (21). In contrast to the present result, the B2-type ordered alloy clusters are obtained being in agreement with the equilibrium phase diagram of Co-Al. These results demonstrate that the nucleation and growth processes of alloy clusters are driven by the thermodynamical alloy phase stability.

## Acknowledgments

The authors wish to thank Dr. T.J. Konno, Dr. M. Sakurai and Dr. S. Yamamuro for valuable comments and technical supports. They are indebted to the Laboratory for Developmental Research of Advanced Materials, Institute for Materials Research, Tohoku University. This work was supported by CREST (Core Research for Evolution Science and Technology) of Japan Science and Technology Corporation (JST) and a Grant-in-Aid for Scientific Research (11450234) given by the Ministry of Education, Science Culture and Sports of Japan.

## References

1. A. S. Edelstein and R. C. Cammarata, Nanomaterials: Synthesis, Properties and Applications, Institute of Physics Publishing, Bristol (1996).
2. H. Gleiter, Prog. Mater. Sci. 33, 223 (1989).
3. R. Uyeda, Prog. Mater. Sci. 35, 1 (1991).
4. P. Melinon, V. Paillard, V. Dupuis, A. Perez, P. Jensen, A. Hoareau, J. P. Perez, J. Tuaillon, M. Broyer, J. L. Vialle, M. Pellarin, B. Baguenard, and J. Lerme, Int. J. Mod. Phys. B9, 339 (1995).
5. H. Haberland, Clusters of Atoms and Molecules I and II, Springer-Verlag, Berlin (1995).
6. W. A. de Heer, Rev. Mod. Phys. 65, 611 (1993).
7. G. Hohl, T. Hihara, M. Sakurai, T. J. Konno, K. Sumiyama, F. Hensel, and K. Suzuki, Appl. Phys. Lett. 66, 385 (1995).
8. S. Yamamuro, K. Sumiyama, M. Sakurai, and K. Suzuki, Supramol. Sci. 5, 239 (1998).
9. S. Yamamuro, K. Sumiyama, and K. Suzuki, J. Appl. Phys. 85, 483 (1999).
10. T. Hihara and K. Sumiyama, J. Appl. Phys. 84, 5270 (1998).
11. H. Haberland, M. Karrais, M. Mall, and Y. Thurner, J. Vac. Sci. Technol. A. 10, 3266 (1992).
12. H. Haberland, M. Mall, M. Moseler, Y. Qiang, T. Reiners, and Y. Thurner, J. Vac. Sci. Technol. A. 12, 2925 (1994).
13. H. Kawamata, Y. Negishi, R. Kishi, S. Iwata, A. Nakajima, and K. Kaya, J. Chem. Phys. 105, 5369 (1996).
14. A. Nakajima, T. Hayase, F. Hayakawa, and K. Kaya, Chem. Phys. Lett. 280, 381 (1997).
15. T. Hihara, S. Pokrant, and J. A. Becker, Chem. Phys. Lett. 294, 357 (1998).
16. S. Sugano and H. Koizumi, Microcluster Physics, 2nd edn., Springer, Heidelberg (1998).
17. H. Mori and H. Yasuda, Mater. Sci. Eng. A217/218, 244 (1996).
18. T. B. Massalski, Binary Alloy Phase Diagrams, 2nd edn., vol. 1, p. 61, ASM International (1990).
19. N. Schönberg, Acta Chem. Scand. 8, 208 (1954).
20. T. Hihara and K. Sumiyama, J. Vac. Sci. Technol. B. in press.
21. T. J. Konno, S. Yamamuro, and K. Sumiyama, in preparation.